Adaptive Measurement for Automated Field Reconstruction and Calibration of Magnetic Systems

Liang Hu, Kok-Meng Lee, *Fellow, IEEE*, Jun Zou, Xin Fu, and Hua-Yong Yang

***Abstract*—This paper presents an efficient method to adaptively determine the locations for taking measurements for automated calibration of electromagnetic systems using reconstructed magnetic fields. This coupled measurement- computation method solves the Laplace's equation with measured boundary conditions. Along with the formulation of two selection criteria (chord-height and data-spacing), an adaptive scanning algorithm has been developed, which bases four local measurements to determine the next measurement point. This adaptive method, which relaxes the assumption of approximately known structure, has been illustrated (with experimental verification) with three practical applications; electromagnetic velocity probe, electromagnetic flow-meter (EMF) and spherical motor. Comparisons against published data demonstrate that the adaptive measurement algorithm greatly reduces the number of measurements and shortens the scanning route length of all three applications without sacrificing the accuracy of the computed results. Dry calibration results of an EMF were also experimentally verified against test data obtained from a standard flow-rig confirming that a relative error of 0.2% can be achieved. This finding makes the cost-effective dry calibration a practical alternative to the conventional flow rig calibration. As demonstrated on a spherical motor, the flexibility to include a least-square curve fit offers a practical means to filter measurement noise.**

***Note to Practitioners*—Motivated by the need for a cost-effective method to replace conventional flow rig calibration of large electromagnetic flowmeters (EMFs), which adds considerably to the product cost, this paper presents an efficient method for improving dry calibration (requiring no actual liquid). This method adaptively determines the points for taking measurements on the boundary surfaces to reconstruct the magnetic field distribution (MFD), and has been experimentally verified on two widely used fluid-to-electrical transducers. As demonstrated experimentally and compared against published data based on gradient method, the adaptive method greatly reduces the number of measurements and length of the scanning route. In addition, the effect of measurement noise on the accuracy of the adaptive method has been investigated on a spherical motor, which illustrates the flexibility to include a least-square fit for filtering measurement noise. While the reconstruction method illustrated here is in the context of electromagnetic fields, the procedure introduced in this paper can be extended to other physical field (such as thermal and electrical) based mechatronic systems, as long as the field obeys similar governing equations (such as Laplace and Poisson equations) with measurable boundary conditions.**

***Index Terms*—Adaptive measurements, automated calibration, flow meter, magnetic field reconstruction, spherical motor, velocity probe.**

I. Introduction

PROFILE reconstruction can be found in many applications which include free-form surface measurement in reverse engineering [1]–[5], vision-based surfaces/volumes reconstruction [6], [7], and more recently magnetic field reconstruction for sensor and actuator calibration [8]–[10]. Reconstruction typically involves two sequential stages; data acquisition and data processing (or computational modeling). Recent advances in computer technology and algorithms have significantly reduced the cost of computational processing once the data are available. Physically accurate reconstructions that rely on a dense set of equally spaced measurements to characterize the profile, however, remain to be time consuming and costly. As will be illustrated in the context of electromagnetic flow-meter (EMF) calibration, adaptive measurements play an important role in improving the time efficiency of automated magnetic field reconstruction.

Increasing competition (among power, irrigation, municipal, industrial, recreation, aesthetic, and fish and wildlife uses) for the finite supplies of water, which is also linked to climate change, energy and food supplies/prices, and troubled financial markets as noted recently in a landmark UN report [11], has motivated better water management. Flowmeters not only help utilities collect the revenue, they also help pinpoint leaks, locate pressure problems along their waterways, and identify and study periods of peak and non-peak use among both residential and business consumers [12]. To assure product reliability and accurately account for water, flow-meters must be accurately calibrated [13]. The electromagnetic methods of measuring flow rates [14] have become more widespread as they are based on one of the accurate laws of physics (the law of electromagnetic induction); their calibration characteristics can be calculated. Conventional flow-rig calibration of large EMFs (with diameter in the order of 1 m), however, is costly and time consuming. It was estimated in [15] that calibrating a 1.2 m-diameter EMF using a conventional flow rig, which

Manuscript received November 01, 2009; revised June 10, 2010; accepted October 11, 2010. Date of publication December 03, 2010; date of current version April 06, 2011. This paper was recommended for publication by Associate Editor S. Sarma and Editor S. Sarma upon evaluation of the reviewers' comments. This work was supported in part by the National Basic Research Program (973) of China (No.2006CB705400), in part by the Key Industrial Program of Zhejiang Province of China (2008C11G2010077), in part by the Zhejiang Provincial Natural Science Foundation of China (No.D1080038), and in part by the Georgia Tech Foundation (2505E34).

L. Hu, J. Zou, X. Fu, and H.-Y. Yang are with the State Key Laboratory of Fluid Power Transmission and Control, Zhejiang University, Hangzhou 310027, China (e-mail: cmeehuli@zju.edu.cn; junzou@zju.edu.cn; xfu@zju.edu.cn; yhy@zju.edu.cn).

K.-M. Lee is with the George W. Woodruff School of Mechanical Engineering, Georgia Institute of Technology, Atlanta, GA 30332-0405 USA. He is also a visiting Pao Yu-Kong Chair Professor, Zhejiang University, Hangzhou 310027, China (e-mail: kokmeng.lee@me.gatech.edu).

Color versions of one or more of the figures in this paper are available online at http://ieeexplore.ieee.org.

Digital Object Identifier 10.1109/TASE.2010.2090654

requires a 250 kW pump to supply water flow of 1.5 tonnes/s, would cost about £3 M, and require between 2 and 4 h to calibrate. The "dry calibration" technique (that requires no actual liquid flow) has been accepted as a cost-effective alternative in the past decade, the key for which is the determination of the magnetic field in the measuring volume. Although magnetic measuring apparatus (such as gauss meter) can measure the magnetic flux density at a point accurately, directly measuring the MFD is cumbersome, because all the three orthogonal components at numerous points need to be measured in a 3D measuring volume. As the absolute calibration factor needs to be established accurately typically to 0.5%, an efficient method to improve dry calibration where error must be within 0.2% or in the same accuracy class with the flow rig calibration [15], remains to be explored.

Recently, a coupled measurement-computation method has been introduced in [10] to obtain the magnetic field distribution (MFD) for dry calibration of electromagnetic EMF and for force/torque calculation and model-based motion control of a spherical motor [16]–[20]. The MFD reconstruction involves solving the Laplace's equation of a magnetic scalar potential with measured boundary conditions (BCs) [10]. This method, which takes advantages of the rapidly advancing computational tools such as finite-element method (FEM), offers two benefits: first, the MFD calibration can be performed without the assumption of known magnetic structures; and measurements are only required on the surface outside the physical regions. Second, it reduces the direct vector measurements of the MFD in 3D space to 2D scalar measurements based on the normal component of the magnetic flux density on the boundary surfaces. In [8]–[10], a dense set of equally spaced measurements was obtained for specifying the necessary BCs. It has been shown that the time required computing the MFD using FEM for calibrating the sensitivity of an EVP or an EMF is in the order of about 5 min. In contrast, measurements for specifying the BCs with an automated scanning mechanism requires several hours. While these high-resolution data provide precise BCs for solving the MFD numerically with FEM and offer benchmark model verification, the measurements are time consuming for practical implementation.

In practice, it is desired to minimize the number of measurements needed to specify the BCs without sacrificing the MFD accuracy computed using FEM. The simplest way is to uniformly decrease the measurements on the whole boundary surface. However, if the BC values are relatively constant in certain local regions, this method is inefficient since extra data in regions of constant values do not help improve the overall calibration but simply prolong measurement time. A better alternative is to base decisions on the BC surface distribution of the magnetic field to select points for measurements. The effect of reduced BC points using the gradient of the reconstructed MFD was explored in [10], showing that a nearly identical MFD (with a relative error of less than 0.15%) can be obtained. This finding, along with the interest to develop a method capable of selecting measured points without any knowledge of the BC morphology, provides the motivation for this paper.

Gradient features have been commonly used to reduce data processing computation; for examples, image compression [21], [22], point interpolation for image improvement [23], FEM mesh refinement [24], and numerical mesh-free computation of magnetic fields [24], [25]. Unlike a typical data processing application which begins with a coarsely resolved base-levels (or regular grids) and follows by refining them based on some specified criterions such as local cell mass and gradient [26], the BC morphology for reconstructing the MFD is usually unavailable during data acquisition. Apart from time required to take measurements, the route length travelled by the scanning probe, which contributes to the nonproductive motion time, must be minimized. Thus, it is desired that the dense BC nodes required for subsequent numerical computation can be interpolated from a small set of appropriately selected data (measured in a single pass) along a shortest scanning route. Similar studies can be found in free-form surface measurements in reverse engineering, where the surfaces are inspected (using tough triggering or laser sensors) with measuring points adaptively determined based on a specified criterion, which may be the change of surface curvature [1], [2], equal arc-length [3], chord height [4], [5], or parameterization based sampling [4] criteria. Among these methods, the chord-height criterion (originally developed for locating feature points in images [27] and extended to free-form surface measurements [4], [5] in reverse engineering) offers several advantages including ease of calculation and sensitive in characterizing curvature changes. The paper extends the chord-height method to determine boundary condition (BC) for magnetic field reconstruction. However, unlike free-form surfaces of a solid geometry, magnetic distributions are vector fields and invisible.

For the above reasons, this paper focuses on developing a set of well defined selection criteria, an adaptive scanning algorithm, and interpolation methods for adaptive measurements requiring no prior information on the BC morphology to avoid round-trips. The remainder of this paper offers the followings.

1) An adaptive scanning algorithm, which determines the locations to take BC measurements for solving the MFD numerically with FEM, is presented. The algorithm uses a small set of nearest calibrated data, along with two well-defined selection criteria, to determine the next measuring point. As will be shown, the flexibility to choose a curve-fit method offers a practical means to handle tradeoff between measurement noise and time.
2) The adaptive method has been applied to two widely used fluid-to-electrical transducers (electromagnetic velocity probe and flow-meter), where high-resolution measurements and published data based on gradient method are available for verification. Comparisons show that the adaptive method greatly reduces both the number of measuring points and the length of the scanning route. Additionally, experimental results comparing the calculated sensitivity of an EMF against direct calibration using a standard flow-rig are also presented, which confirm the cost-effectiveness of the dry calibration with reconstructed magnetic fields.
3) The effect of measurement noise on the accuracy of the adaptive method has been investigated using published data of a spherical motor [17]. Two different curve-fit methods (cubic-spline and least-square) are chosen for

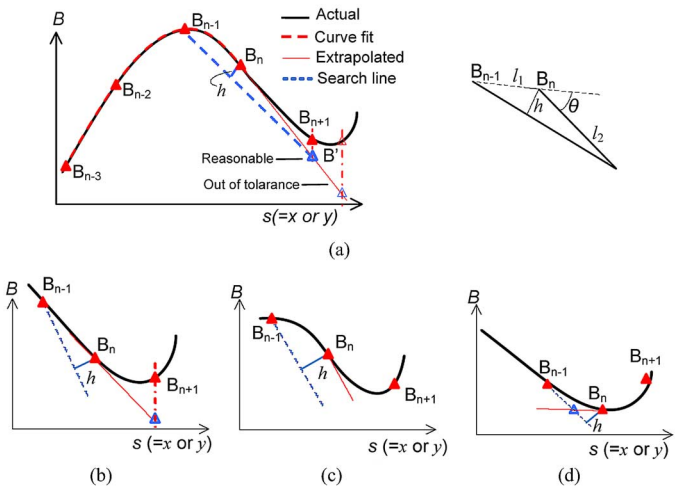

Fig. 1. Schematics illustrating chord-length criterion.

this study. Unlike a cubic-spline fit, least-square fits do not require the curves to pass through the noisy measurements, and thus noise is effectively "filtered."

Once the MFD is reconstructed, the flow velocity of EMF and EVP can be determined from the Faraday's law of electromagnetic induction [14]. Similarly, with the known MFD the torque model of the spherical motor can be computed from the Lorentz force law [16]–[18]. Thus, this paper focuses on developing a method to efficiently obtain measured BCs for solving the MFD.

II. Adaptive Algorithm

In physics, any potential field ψ obeying Laplace's equation is free and can be uniquely determined by the field conditions on the boundary surface. Mathematically, the magnetic flux density $\mathbf{B}$ in a source-free space can be solved from the Laplace's equation

$$\nabla^2\psi = 0 \tag{1a}$$

and

$$\mathbf{B} = -\mu\nabla\psi \tag{1b}$$

where μ is the magnetic permeability of the material in the working space. As reported in [10], the source-free MFD can be reconstructed from measured flux density on its boundary surface using FEM. High fidelity reconstruction often requires a sufficiently large number of nodes. The tradeoff, however, is measurement cost since fewer points imply less time needed. In order to reduce cost, it is desired that the required dense BC nodes can be interpolated from a small set of measurements. Appropriate selection of characteristic data along a shortest scanning route requires a set of well defined selection criteria, an adaptive scanning algorithm, and interpolation methods.

A. Selection Criteria

The scalar component of the flux density on a point in 2D region can be expressed as $B(x, y)$ or in discrete form $B(i, j)$. As will be illustrated, the scanning route considered here is a path parallel to the x or y axis. As illustrated in Fig. 1, the four

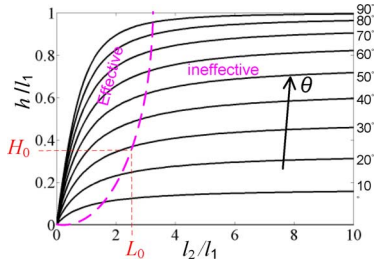

Fig. 2. Effect of changing curvature on chord-height.

nearest calibrated data (B_{n-3}, B_{n-2}, B_{n-1}, and B_n) provide a basis to determine the next measuring point along a path (in the x or y direction). With the data curve-fitted using method such as cubic spline or least-square, the next measurement B_{n+1} can be taken at a point extrapolated from B_n along its tangent. An appropriate point for the next measurement can be determined as follows.

To begin with, a search line (originated from the previous measurement B_{n-1}) is introduced, which intercepts the B_n-tangent line. Next, a selection criterion can be defined quantitatively in terms of a chord-height h and normalized data-spacing $L = l_2/l_1$ (Fig. 1), where l_1 and l_2 are the straight-line distances between B_{n-1} and B_n, and between B_n and the searched point on the B_n-tangent line. As illustrated in Fig. 1 and given mathematically by (2), the chord-height h is the perpendicular distance from B_n to the search line from B_{n-1}

$$H = \frac{h}{l_1} = \frac{L\sin\theta}{\sqrt{1 + L^2 + 2L\cos\theta}} \text{ where } L = \frac{l_2}{l_1} \tag{2}$$

where θ is the angle between the B_n-tangent line and the straight line connecting B_n and B_{n-1}. For $-\pi/2 \le \theta \le \pi/2$, the sign of H depends on $\sin\theta$ since cosine is an even function and hence the denominator of (2) is always positive. Additionally, $H \to \sin\theta$ when L is much larger than unity. Equation (2) is graphed in Fig. 2 to illustrate the effect of the normalized data-spacing $L = l_2/l_1$ and changing curvature θ of B (with respect to x or y) on the chord-height. As shown in Fig. 2, H provides a simple criterion to compare the "degree" of the local (or surface) curvature but is insensitive to L (when $L > 3$). A single selection criterion based solely on chord-heights would tend to miss local maxima or minima (as illustrated in Fig. 1), and result in undesirably low density samples. Thus, the selection of measuring points involves two independent thresholds:

- chord-height threshold, H_o;
- data spacing threshold, L_o.

A common technique to locate the point for taking the next measurement along the B_n-tangential line is to rotate the search line about (s_{n-1}, B_{n-1}) incrementally until $H \approx H_o$ where the chord-height at different extrapolated points can be calculated from the calibrated nodes, (s_{n-1}, B_{n-1}) and (s_n, B_n) using (3)

$$h = \frac{\left|\left[m_n\Delta s_{n+1} + \Delta B_n\right]\Delta s_n - \left(\Delta s_{n+1} + \Delta s_n\right)\Delta B_n\right|}{\sqrt{\left[m_n\Delta s_{n+1} + \Delta B_n\right]^2 + \left(\Delta s_{n+1} + \Delta s_n\right)^2}} \tag{3}$$

where $\Delta s_n = s_n - s_{n-1}$; $\Delta B_n = B_n - B_{n-1}$; and m_n is the slope of the B_n-tangent line. In (2), s could be x or y, as shown in Fig. 1.

Alternatively, L (and hence the point for taking the next measurement) can be inversely solved for a specified H_o in terms of θ from (2) which can be written as

$$L^2 - 2bL - c = 0 \tag{4}$$

where $b = H_o^2 \cos\theta/(\sin^2\theta - H_o^2)$; $c = H_o^2/(\sin^2\theta - H_o^2)$; and $\sin\theta \neq H_0$. When $\sin\theta \leq H_0$, there is no practical solution for $L > 0$ since the B_n-tangent and search lines could be in parallel, overlap or intersect but with $L < 0$

$$\sin\theta \begin{cases} = 0, & \text{lines overlap, Fig. 1(b)} \\ = H_0, & \text{lines parallel, Fig. 1(c)} \\ < H_0, & \text{lines intersects with } L < 0, \text{Fig. 1(d)} \end{cases}.$$

When $\sin\theta > H_o$ as illustrated in Fig. 1, the lines intersect at a potential search point that a practical solution ($L > 0$) to (4) can be solved from (5)

$$L = b + \sqrt{b^2 + c}. \tag{5}$$

In either (3) or (5), if $L > L_o$, L is equal to L_o. Equation (5) illustrates intuitively the relationship among the chord height h, the angle θ characterizing the curvature change, and the straight-line distance l_2. When scanning automatically, the sensor is mechanically positioning in terms of step size Δs along s. Thus, the data spacing threshold during real-time scanning is specified in terms of step size Δs, or $DS = n(\Delta s)$.

The adaptive scanning algorithm aims at minimizing the number of steps without sacrificing fidelity; in other words, characterizing key features, particularly around curvatures, for high-fidelity reconstruction of the magnetic field. Thus, when $\sin\theta = 0$ (data on a straight line) or $\sin\theta = H_0$ (immediately after a local maxima or minima), the next location for taking measurement is selected with the largest data spacing DS. Once the actual B_{n+1} is measured, the derivatives of the curve-fit B function are then checked for any sign change from B_n and B_{n+1}. If a sign change is detected implying that a local maxima or minima could be missed as illustrated in Fig. 1(b) and (c), additional measurements (at regular intervals between B_n and B_{n+1}) should be made to improve fidelity around the local maxima or minima. When $\sin\theta < H_0$ indicating a change in curvature, B_{n+1} is measured at the next nearest interval to avoid skipping a local maxima or minima as illustrated shown in Fig. 1(d) . These cases ($\sin\theta \leq H_0$) are illustrated in Fig. 1.

B. Adaptive Scanning Algorithm

Fig. 3 provides an overview of the scanning algorithm, which scans along increasing y then decreasing y in specified increments of x. The measurement steps are as follows.

Step 1) *Scan along y with constant incremental x [Fig. 3(a)].*
- a) The scan begins (at $i = 1$) with four initial (equally spaced Δy) measurements to provide a curve-fit (using method such as cubic spline or least-square).
- b) Determine the next measuring point based on the selection criteria (H_o, L_o). Using (5), L is calculated. If $L > L_o$, L is equal to L_o. The corresponding y_{n+1} is calculated.
- c) The actual value B_{n+1} is measured at y_{n+1}.

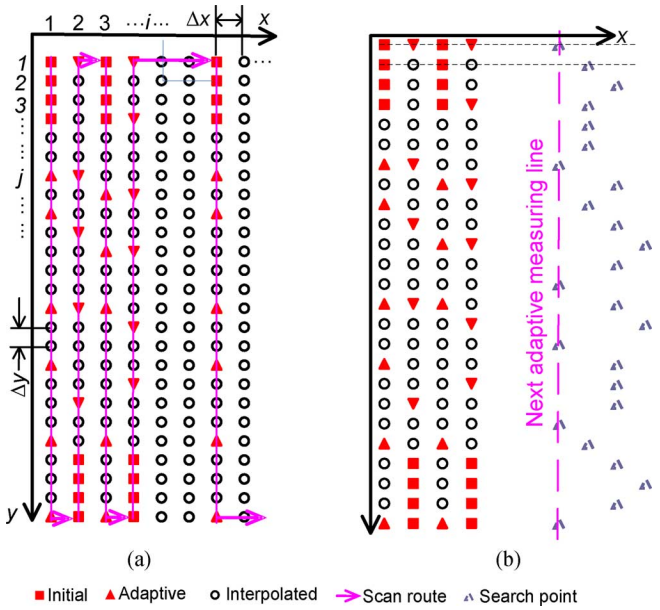

Fig. 3. Illustration of the adaptive measuring process.

- d) Values of the unmeasured (equally spaced) nodes are then interpolated from the measured points.
- e) Using the four latest nodes, steps 1a–1c are repeated until all nodes in regions ($1 \leq i \leq 4$, y) are measured or interpolated.

Step 2) *Scan along x with incremental y [Fig. 3(b)].*
- a) For each constant-y row, the next measuring point along x is determined from the measured or interpolated nodes using the same criterion (as in Step 1b but with y replaced by x).
- b) Since Step 2a could result in different i values for different j, the minimum i value (or $i_{\min}$) is selected to begin the new scanning route.
- c) Steps 1a–1c are repeated and unmeasured nodes before $i_{\min}$ column are interpolated.

Steps 1 and 2 are repeated until all the nodes on the BC surface are specified.

C. Practical Implementation Considerations

To investigate the effectiveness of the adaptive selection method, an adaptive algorithm has been written in Matlab to provide a basis for comparing the effect of measurement noise and time on the choice of a curve-fit method. Two methods are chosen for illustration; cubic-spline and least-square fits.

Tested on a PC (with 2.8 GHz CPU and 512 MB RAM), the cubic-spline-fit takes about 6 ms, while the least-square-fit requires 10 ms; both use a cubic polynomial as a base shape function. The time for these curve-fits, however, is negligible when compared against the measurement time in the order of 0.5 to 1 s per point.

Cubic-spline fits are susceptible to measurement noise as the curves must pass through measured points. If the noise-to-threshold is significant, the next measuring position based on the cubic-spline-fit will be erroneous. Through a properly selected base-shape function, a least-square fit can

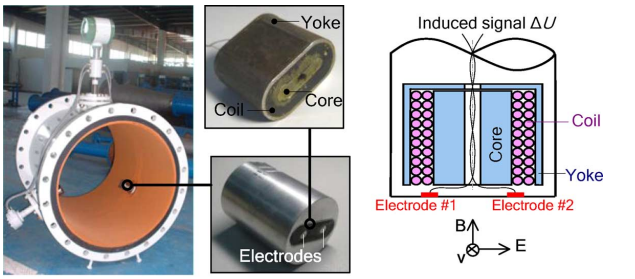

Fig. 4. EVP Schematics, principles, and applications. (a) Tri.-EVPs measuring system. (b) Illustration.

effectively "filter" noise. The tradeoffs are that the least-square fitting is more computational demanding (than the cubic spline fitting), and that the selection of a suitable base shape function may not be easy.

III. Validation and Verification

Two widely used fluid-to-electrical transducers (based on Faraday's induction law), the electromagnetic velocity probe (EVP) and the EMF, are chosen here as illustrative examples, where published data are available as a basis for verification. The rule-of-thumbs for selecting the thresholds are as follows. The chord-height (CH) threshold is specified in terms of the maximum B value on the BC surfaces. To determine this value, a quick scan using a Gauss-meter is made before taking adaptive measurements in real time. In the two studies discussed here, the Max Hold function in the Gauss-meter (Lakeshore Model 421) is used, which continuously searches for and registers the largest B value during the quick scan without stopping. The time needed to complete the quick scan is short; for the EMF, the process takes less than 3 min. The data-spacing (DS) threshold is defined as a number of Δs (where Δs is node-spacing or step-size along the x or y direction) according to Shannon's sampling theorem in equal-spaced methods [8]–[10].

In both these examples, the CH threshold equals to 1% of the maximum B values (about 10 G and 100 G on the side and end BC surfaces of EVP, and 20 G on the BC surface of EMF, respectively). The DS threshold is $3(\Delta s)$; the step-sizes are 1 mm, 3°, and 2 mm in ρ, θ, and z directions, respectively.

For verifying the reconstruction based on the adaptive selection (AS) method, we define the reconstruction error ΔB relative to a set of high-resolution (HR) data

$$\Delta B = \frac{(B|_{\mathrm{AS}} - B|_{\mathrm{HR}})}{B|_{\mathrm{HR}}} \tag{6}$$

where the subscripts, AS and HR, refer to the adaptive selection method and the high-resolution data, respectively.

A. Adaptive BC Measurement for Solving MFD of EVP

Fig. 4 shows the EVP for measuring the flow-rate of the fluid through a large pipe, where a voltage signal ΔU is induced between the electrodes (in the probe consisting of an EM coil with ferrous core and yoke) when conductive liquid (with velocity $\mathbf{v}$) flows through the magnetic field $\mathbf{B}$ of the EM coil. In [9], the MFD around the EVP was reconstructed for dry calibration

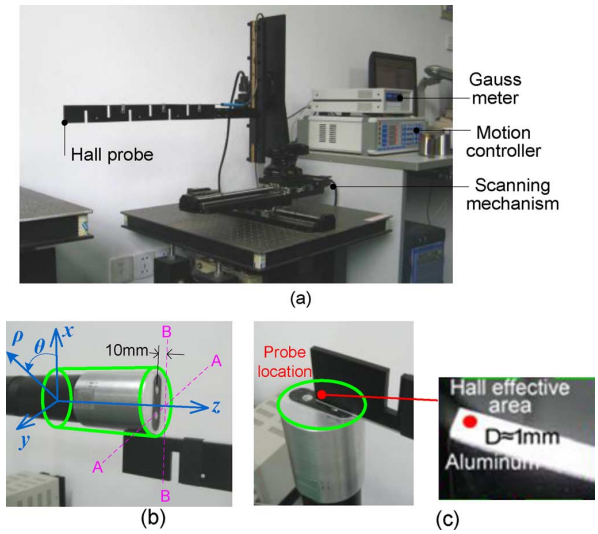

Fig. 5. Experimental setup. (a) Experimental setup. (b) Side surface. (c) End surface.

TABLE I
Parameters Used in Adaptive Selection

	Side		End	
	θ	z	θ	ρ
CH threshold	0.1G		1G	
DS threshold	9°	6mm	9°	3mm
Step size	3°	2mm	3°	1mm
Scan Area	[0,360°]	[0,220mm]	[0,360°]	[0,30mm]

using the experimental setup in Fig. 5, where the normal component of the flux density passing through the electrode-end and side surfaces was measured. The reference coordinate system is defined on the plane at 210 mm from the end surface (with its x axis parallel to the line connecting the two electrodes, and the z axis along the coil centerline). Correspondingly, the MFDs for the end and side surfaces in cylindrical coordinates are denoted as $B(\theta, \rho)$ and $B(\theta, z)$. A dense set of equally spaced measurements (in steps of 1 mm, 3°, and 2 mm in ρ, θ, and z directions, respectively) on the side and end surfaces of the probe were obtained in [8]. For the purpose of comparison, the same step sizes are used here. The selection criteria for the adaptive algorithm are summarized in Table I.

As shown in Fig. 5, the computer-controlled scanning servo mechanism (designed to automate data collection and ensure a high measuring accuracy) positions the Hall probe (mounted on the aluminum holder). Fig. 6 and Table II summarize the distribution of the measurement points (MP), where the color of the points corresponds to that of the measured magnetic flux density in Fig. 7. Since the structure is symmetric and the corresponding fields are similar (though generally not identical in practice), only half of the regions are plotted in Fig. 7.

For each of the BC surfaces, the probe scans along the θ direction for each increment of ρ or z. As an illustration, Fig. 7(a) shows the first scan-route from ($\theta = 0$, $\rho = 1$) to (360°, 1), the second from (360°, 2) to (0°, 2), then the third from (0°, 3) to (360°, 3), etc.; each path begins with four initial measurements. Because the end-surface measurements form a relatively smooth profile [Fig. 7(a)], most of the MPs in Fig. 6(a) are uniformly spaced with an interval equal to the DS thresholds of 9°

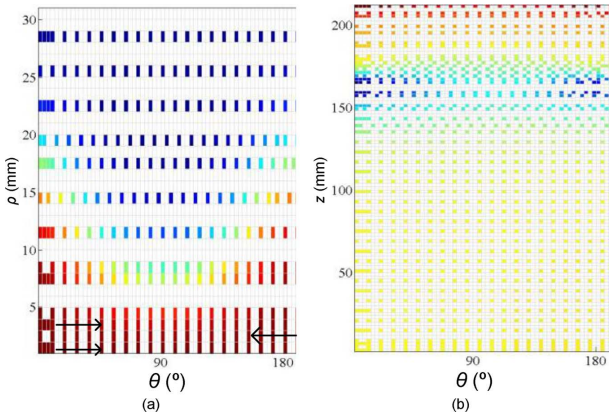

Fig. 6. Measurement point distribution. (a) End surface MP. (b) Side surface MP.

TABLE II
MEASURING POINTS (MP), DISTANCE TRAVELED AND TIME

	Adaptive selection		High resolution [1]	
	Side	End	Side	End
# of MP	1,861	549	12,600	3,580
Route length (mm)	9,065	960	20,180	2,920
Time (min)	21	6	140	30

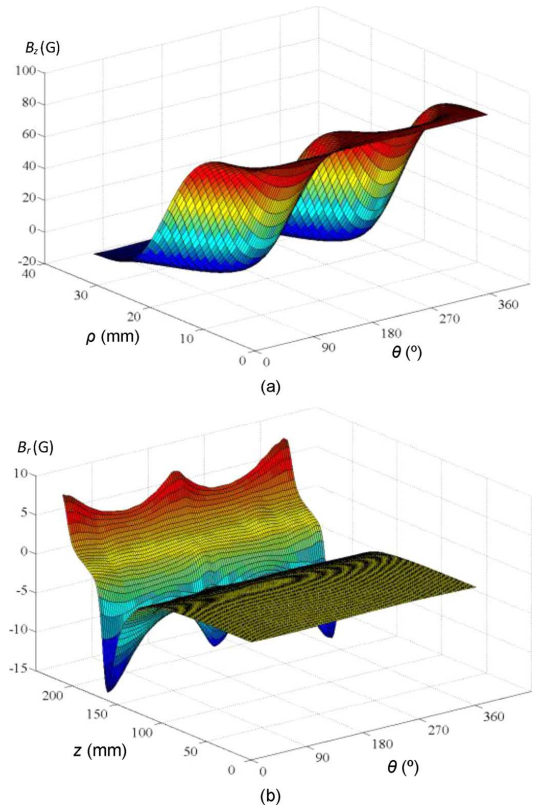

Fig. 7. Adaptive BC measurements of the EPV. (a) Measured BC on end surface. (b) Measured BC on side surface.

and 3 mm. For the side surface, the point distribution in Fig. 6(b) is relatively sparse except the four initial MPs in each row and in regions ($z > 130$ mm), where the coil, yoke, and core are located; the findings are consistent with Fig. 7(b) as expected.

The reconstructed normal component of the flux density and their relative errors are summarized in Figs. 8 and 9, where ΔB is defined in (5) with HR referring to the high-resolution data published in [1].

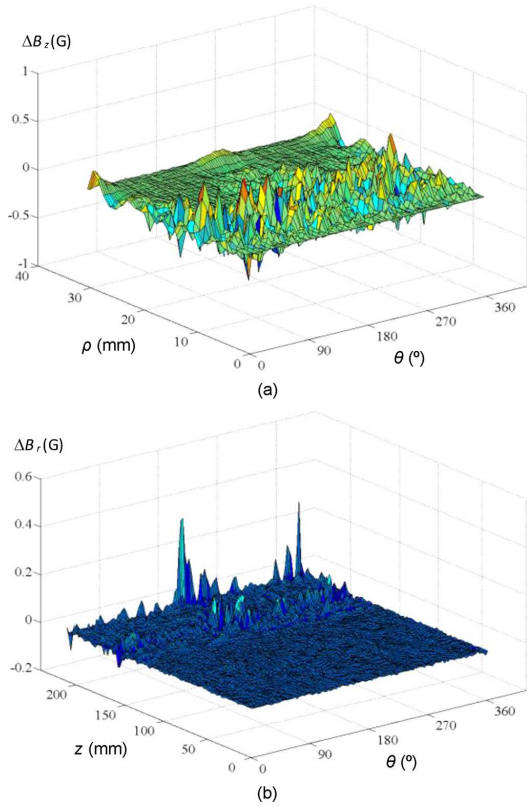

Fig. 8. Relative errors of adaptive method for EVP. (a) Relative error of the normal flux density on the end BC surface. (b) Relative error of the normal flux density on the side BC surface.

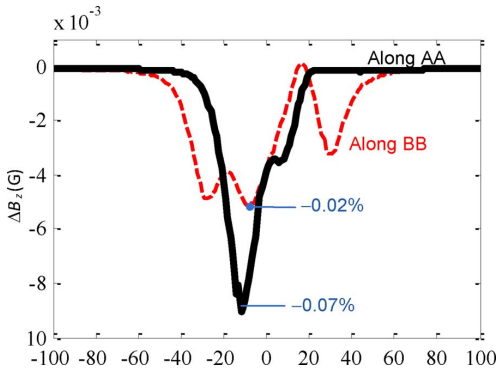

Fig. 9. Relative error of reconstructed along AA and BB.

In Fig. 9, measurements are along the AA and BB lines [parallel to x and y axes on a plane 10 mm from the end surface in Fig. 5(b), respectively]. The relative errors of the reconstructed B_z are less than 0.1%. Maximum errors occur primarily at local maxima and minima. As compared in Table II, the adaptive selection algorithm requires only 1/7 of the original HR measurements [8] (or 15%~20% of the measuring time) for reconstructing the MFD with the same resolution. Note that measuring time is approximately linearly proportional to MP.

B. Dry Calibration of EMF With Flow

Fig. 10 shows an EMF for determining the flow rate by measuring the magnitude of the voltage ΔU (induced across the

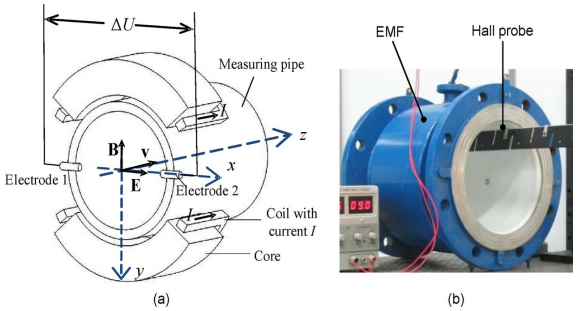

Fig. 10. Schematics illustrating the measurement of EMF BC (adapted from [10]). (a) EMF with inner U-shaped electromagnets. (b) Experimental measurement of BC.

TABLE III
STRUCTURE CHARACTERISTICS OF THE EMF (DIMENSIONS IN MM)

Pipe	Average diameter, length	201.05, 340
Electrodes	Diameter, distance apart	10.18, 197.57

two electrodes) as conductive liquid in the pipe flows through the magnetic field of the U-shaped electromagnets. The induced voltage ΔU is a function of the average flow velocity v and the magnetic flux density B. Through measuring the magnitude of the induced voltage, the flow velocity can be determined from the Faraday's law of electromagnetic induction [14].

EMFs must be calibrated to establish a sensitivity factor for each unit, and are conventionally calibrated in flow rig. To reduce cost for calibrating large EMFs, dry calibration has been widely explored as a potential alternative. For practical implementation, dry calibration must be efficient with precision in the same accuracy class of flow rig calibration [15]. As a basis for evaluation, results of dry calibration on the EMF (Fig. 10) based on the reconstructed magnetic field are verified against data obtained using a standard flow-rig setup. The characteristic dimensions of this EMF are listed in Table III.

1) Principle of Dry Calibration: The sensitivity S of the EMF to be calibrated is defined in (7)

$$S = \frac{\Delta U}{\overline{v}} \tag{7}$$

where ΔU is the induced voltage between two electrodes; and $\overline{v}$ is the average flow velocity passing through the measuring pipe (with radius r). As introduced in [8] and [14], the induced voltage ΔU can be calculated according to

$$\Delta U = \int_{\Omega} \mathbf{v} \cdot (\mathbf{B} \times \mathbf{W}) d\Omega \tag{8}$$

where Ω is the measuring volume; and the weight function $\mathbf{W}$ (that characterizes the contribution of the induced voltage to the output signal via the electrodes at different positions in the volume) can be determined in term of the Green's function G defined in (8)

$$\mathbf{W} = \nabla G; \tag{9a}$$

$$\nabla^2 G = 0; \tag{9b}$$

$$\left.\frac{\partial G}{\partial \rho}\right|_{\rho=r} = \begin{cases} \delta & \text{electrode} \\ 0 \end{cases} \tag{9c}$$

TABLE IV
COMPARISON BETWEEN ADAPTIVE AND GRADIENT-BASED METHODS. (STEP SIZE: 3° FOR θ; AND 2 mm IN z; RANGE: $0 \le \theta \le 360°, 0 \le z \le 300$ mm)

	Adaptive Thresholds: CG = 0.2G; $DS_\theta = 9^o$; DS_z =6mm	Published data [10] Gradient-based	Published data [10] High resolution
# of MP	2,725	4,526	18,000
Route length (mm)	37,680	125,600	188,400
Time (min)	27	45	180

where δ is the delta function.

For specified geometry (and hence measuring volume Ω) and electrode positions given in Table IV, the weight function $\mathbf{W}$ can be determined from (9). With this information along with assumed uniform unit flow velocity v ($= 1$ m/s) for fully developed turbulent flow, the sensitivity S can be numerically calculated from (7) once the magnetic field B in the measuring volume of the EMF is reconstructed from the solution to (1) with measured BCs.

2) Comparing Adaptive Against Gradient-Based BCs on MFD: For dry calibrating the EMF sensitivity, the MFD in the pipe is reconstructed with the aid of FEM where the measured flux density on the cylindrical surface is specified as BCs. Based upon the assumption that commercial EMFs have similar structures (and thus similar MFD) obeying common design criteria developed over the past decades, a gradient-based method for reducing measurement points was investigated in [10], where a (high-resolution) set of equally spaced measurements is also available for a benchmark comparison. The interest here is to evaluate the adaptive selection method (that does not require prior knowledge of the inner magnetic structure) against the gradient based method. For comparison, published high-resolution measurements [10] are used to compute ΔB defined in (6).

As for the EPV, the probe (Fig. 10) scans along θ (or circumferentially) for each z increment based on selection criteria summarized in Table IV. The MP distribution and reconstructed B_r using the adaptive selection method are graphed in Fig. 11. The comparisons against the gradient-based method are given in Fig. 12 and Table III. As compared in Fig. 12, the errors (relative to the high-resolution data) of both adaptive and gradient-based methods are similar. The maximum error is about 0.2 G (or 1% of the maximum BC value). However, the adaptive selection method not only requires only 3/5 of the MPs and time used in the gradient-based method, but also relaxes the assumption of approximately known structure.

3) Experimental Flow-Rig Setup: Fig. 13 shows the large flow-rig setup for experimentally verifying the dry calibration of the EFM using the reconstructed MFD. The EMF being calibrated is installed between two long straight pipes (to ensure the flow passing through the EMF is fully developed during calibration). Water flow at steady state is supplied by a high-power pump along with an underground water reservoir and a tall water tower that serves as a constant water-level (and hence pressure head) buffer tank. This setup provides a basis to determine the precision of the EMF by comparing the total water volume measured by the EMF for a specified period of time against the actual volume accumulated in the standard metal tanks.

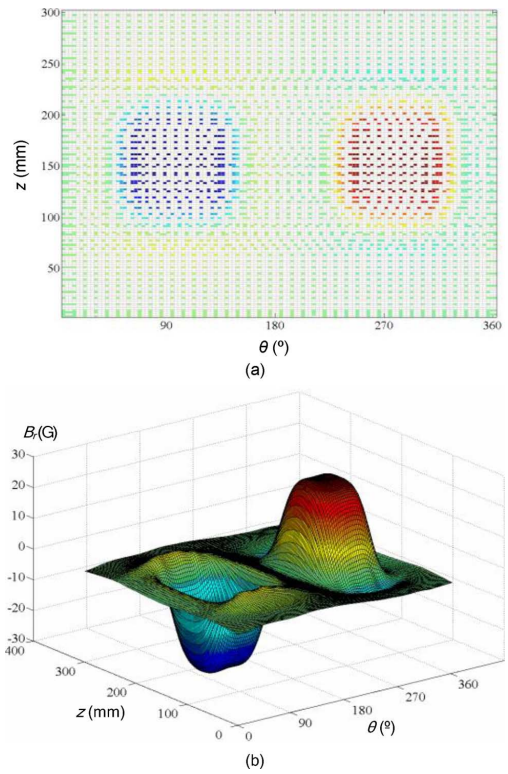

Fig. 11. Measurement point distribution and reconstructed MFD. (a) MP distribution as adaptively measuring BC. (b) Adaptively measured BC.

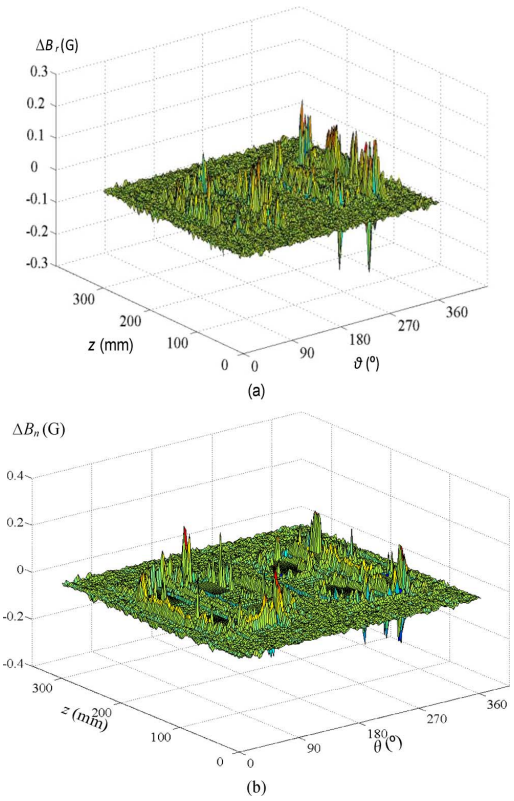

Fig. 12. Comparison of relative errors (EMF). (a) Adaptive selection method. (b) Gradient-based method.

With this flow-rig setup, the values of the EMF sensitivity at three different flow rates ($Q = 50$, 250 and 500 m^3/h which correspond to Reynolds numbers of 8.84×10^5, 4.42×10^6 and 8.84×10^6) are measured. For the turbulent water flow, the fully developed velocity profile is expected to be relatively uniform. Two readings for each flow-rate were taken. The average value of the measured S is used as a standard value to evaluate the precision of the dry calibration.

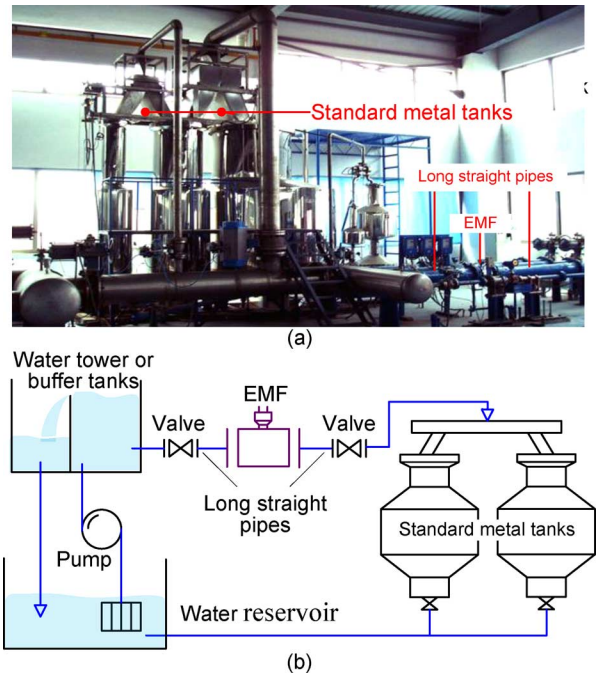

Fig. 13. Flow-rig setup. (a) Flow-rig experimental setup. (b) Illustration of the setup.

TABLE V
COMPARISON OF DRY CALIBRATION AND FLOW-RIG CALIBRATION

Sensitivity	Dry calibration			Flow-rig calibration (average based on Q=50, 250, 500m^3/h)
	Adaptive	Gradient-based	High resolution	
mV/(m/s)	0.11088	0.11087	0.11090	0.111095
% error	−0.193	−0.203	−0.176	
Time (h)	1	1.25	4.5	1.5

4) Results and Discussion: Table V compares the sensitivity of the dry calibrated EFM using three different sets of measured BC data for reconstructing the MFD; namely, adaptive, gradient based and high-resolution measurement [10]. The % errors of dry calibration are computed relative to the direct experimental flow-rig calibration, all of which are about -0.2%. This close agreement validates the method of using adaptive BC measurements to reconstruct the magnetic field for dry calibration.

It is worth noting that the adaptive method achieves the same precision as that using high-resolution data but requires less than 25% of its calibration time. The reduced measurements greatly enhance the efficiency of dry calibration with a negligibly small error (0.017%) in reconstructed MFD. This finding makes the dry calibration a practical, cost-effective alternative to the conventional flow rig calibration.

The small relative error in the dry calibration could be due to the uniform velocity assumption, which neglects the fluid boundary layers covering the surfaces of the measuring pipe and electrodes. Introducing hydrodynamics (taking into account of

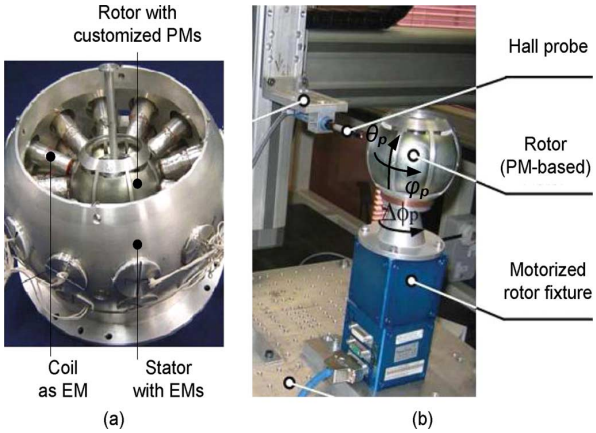

Fig. 14. Spherical motor and measurement setup [17]. (a) Spherical motor. (b) Measuring device.

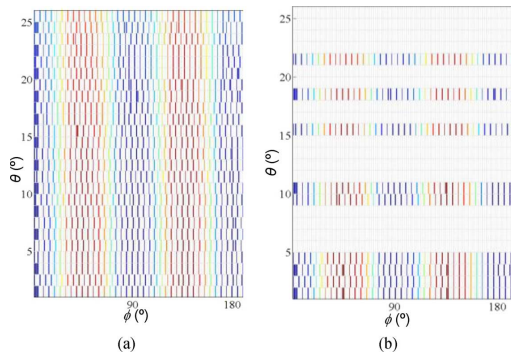

Fig. 15. Adaptively selected measurement points. (a) Cubic-spline fit. (b) Least-square fit.

unmodeled flow effects into calculation) may further improve the precision of dry calibration, which could be an interesting topic for future study.

IV. Effect of Measurement Noise (Spherical Motor)

When the noise-to-threshold is high, the cubic-spline fitting could reduce the effectiveness of the adaptive selection method. Alternative curve-fit methods (such as least-square fitting) capable of filtering noise should be used. As an illustration, we investigate the effect of two different curve-fit methods, cubic-spline (CS) and least-square (LS), on the adaptive selection algorithm using published measurements [17] for reconstructing the MFD of a spherical motor. Reconstructing the rotor MFD (essential for determining the orientation and predicting the torque of the spherical motor) provides an effective means to compensate for manufacturing uncertainties. More details using the MFD for design, measurement, and control of a spherical motor can be found in [16] and [18] .

As shown in Fig. 14(a), the spherical motor consists of an assembly of permanent magnets (PMs) embedded in the spherical rotor, which rotates as appropriately controlled currents flow through the stator coils in the MFD of the PMs. Fig. 14(b) shows the experimental setup [17] for measuring the magnetic flux density at the rotor surface, where the Hall-probe circumferentially scans (in the ϕ direction) for each θ increment as the motorized fixture spins the spherical rotor about its own axis. The selection criteria and MP distribution obtained using two fitting

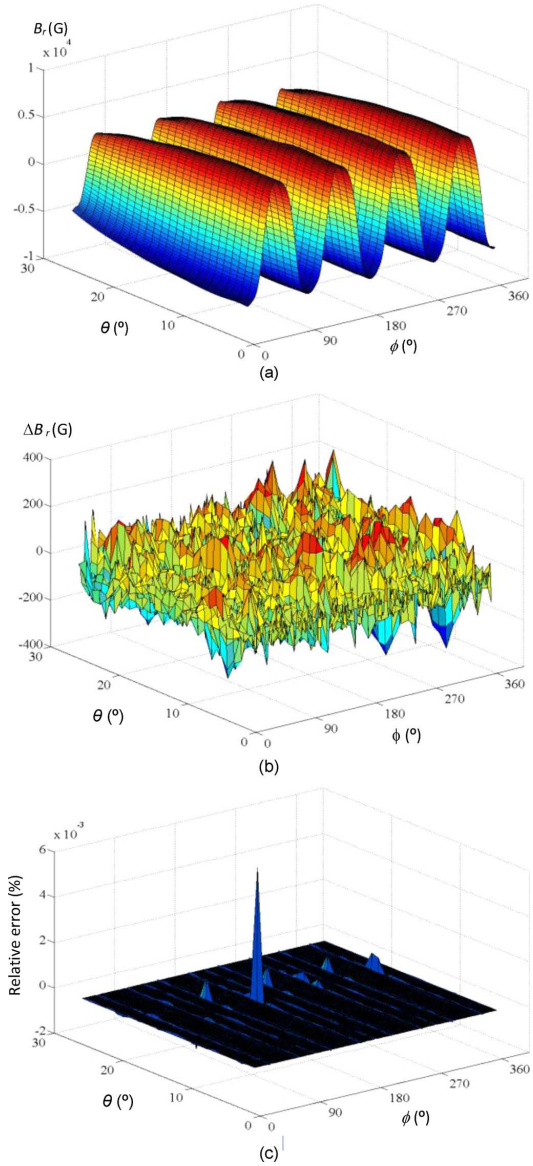

Fig. 16. Relative error of LS-based adaptive selection (spherical motor). (a) Cubic-spline fit. (b) Least-square fit. (a) Reconstructed BC using LS-based adaptive selection. (b) Relative error between LS-based selection and measured data. (c) Relative error of reconstructed B_r at $d_a = 2.5$ mm.

TABLE VI
Selection Criteria and Comparison (MFD of a Spherical Rotor)
(Step Size: $\Delta\theta = \Delta\phi = 1°$; Range: $0 \le \theta \le 25°, 0 \le \phi \le 360°$)

AS thresholds: CG = 10G; DS_θ= DS_φ =5°	**Curve-fit method**		**High resolution**
	CS-fit	**LS-fit**	**[10]**
# of MP	1,906	733	9,360
Route length (mm)	7,432	2,573	7,432

methods are compared in Table VI and Fig. 15; only one-half of the scanning area is shown for the symmetrical rotor structure. The reconstructed MFD (using the LS-based selected points) for specifying as BCs and its relative error are given in Fig. 16.

Figs. 15 and 16 offer some insights to the effects of the measurement noise on the adaptive measurements.

- Fig. 16(b) plots the difference between the reconstructed MFD (using the LS-based selection) and the original measured data. The error map suggests that the measurement

noise-to-threshold ratio is on the order of approximately 10. As a result, noisy measurements cause the CS-based algorithm to scan every θ-row with points uniformly spacing equal to the DS threshold, as shown in Fig. 15(a).

- Unlike a CS fit, the LS fit (based on quadratic polynomials here) does not require the curves to pass through the noisy measurements; noise is effectively "filtered." Fig. 15(b) shows that the LS-based selection requires only 9 of the 25 θ-rows and thus shortens the scanning route by 40%. As compared in Table VI, only 40% of the measurement points for the CS-based adaptive method (or 8% of the original high-resolution data) are needed in the LS-based selection. These savings are a direct result of skipping the 16 of the 25 θ-rows where changes in B_r along θ are negligibly small.
- To further investigate the effect of the LS-based adaptive selection method on the reconstruction accuracy, the Laplace's (1) along with the far-field BCs and the BC specified in Fig. 16(a) is numerically solved using Comsol, a commercial FEA package. Fig. 16(c) compares the reconstructed $B_r(\theta, \phi)$ against published experimental data at 2.5 mm from the surface of the spherical rotor; the relative error is within 0.005%.

V. Conclusion

An adaptive method to reconstruct the magnetic field using a small set of scalar measurements for specifying the BCs has been presented for automated calibration of electromagnetic devices. This method (based on four latest measured data to determine the location to take next measurement) has been applied (with experimental verification) to three applications; EVP, EMF, and spherical motor. The agreement between dry calibration and flow-rig experiment is within 0.2% error.

Comparisons against published data on EMF [10] demonstrate that the adaptive measurement algorithm greatly reduces the number of measurements to 1/7 and shortens the scanning route length to 1/5 from the original high-resolution data without sacrificing the accuracy of the computed results. The adaptive selection (based on chord-height and data-spacing thresholds) not only requires 3/5 of the measuring points and time as compared to the gradient-based method in [10], but also relaxes the assumption of approximately known structure. Similar time savings were experimentally confirmed in the EVP and spherical motor applications. In addition, the flexibility to include a least-square fit offers a practical means to filter measurement noise as demonstrated in the MFD reconstruction of the spherical motor.

While the adaptive method is illustrated here in the context of automated MFD reconstruction, it can be extended to automated calibration of other physical quantities such as electrical, thermal and mechatronic fields. Furthermore, as chord-height criteria have been demonstrated in image processing [27] as well as free-form surface measurements [4], [5] this method can be extended to characterize BC of devices where surface geometry is not available by integrating techniques developed for free-form surface measurements and/or image processing.

References

[1] M. Koster, "Curvature dependent parameterization of curves and surfaces," *Comput. Aided Design*, vol. 23, no. 8, pp. 569–579, 1991.

[2] Y.-J. Liu, Y.-K. Lai, and S. Hu, "Stritification of free-form surfaces with global error bounds for developable approximation," *IEEE Trans. Autom. Sci. Eng.*, vol. 6, no. 4, pp. 700–709, Oct 2009.

[3] J. Hu, Y. Li, Y. Wang, and J. Cai, "Adaptive sampling method for laser measuring free-form surface," *Int. J. Adv. Manuf. Technol.*, vol. 24, no. 11–12, pp. 886–890, 2004.

[4] I. Ainsworth, M. Ristic, and D. Brujic, "Visual CAD-based measurement and path planning for free-form shapes," *Int. J. Adv. Manuf. Technol.*, vol. 16, no. 1, pp. 23–31, 2000.

[5] H. Park, "A solution for NURBS modelling in aspheric lens manufacture," *Int. J. Adv. Manuf. Technol.*, vol. 23, no. 1–2, pp. 1–10, 2004.

[6] S. M. Bhandarkar, X. Luo, R. F. Daniels, and E. W. Tollner, "Automated planning and optimization of lumber production using machine vision and computed tomography," *IEEE Trans. Autom. Sci. Eng.*, vol. 5, no. 4, pp. 677–695, Oct. 2008.

[7] Y. Cheng and M. A. Jafari, "Vision-based online process control in manufacturing applications," *IEEE Trans. Autom. Sci. Eng.*, vol. 5, no. 1, pp. 140–153, Jan 2008.

[8] L. Hu, J. Zou, X. Fu, Y. H. Yang, X. D. Ruan, and C. Wang, "A reconstruction approach to determining the magnetic field around an electromagnetic velocity probe," *Meas. Sci. Technol.*, vol. 20, no. 1, p. 05103(7pp), 2009.

[9] X. Fu, L. Hu, J. Zou, H. Y. Yang, X. D. Ruan, and C. Y. Wang, "Divisionally analytical reconstruction of the magnetic field around an electromagnetic velocity probe," *Sens. Actuators A: Phys.*, vol. 150, no. 1, pp. 12–23, 2009.

[10] L. Hu, K.-M. Lee, and X. Fu, "A method based on measured boundary conditions for reconstructing the magnetic field distribution of an electromagnetic mechatronic system," *IEEE/ASME Trans. Mechatronics*, vol. 15, no. 4, pp. 595–602, Aug. 2010.

[11] The Water in a Changing World, *United Nations World Water Development Report 3*, 2009.

[12] *Water Measurement Manual* United States Department of the Interior Bureau of Reclamation, Water Resources Research Laboratory, Government Printing Office. Washington, DC, Reprint, 2001.

[13] *Water Meter Calibration, Repair, and Replacement Program, EPD Guidance Document* Georgia Environmental Protection Division Watershed Protection Branch, 2007.

[14] J. A. Shercliff, *The Theory of Electromagnetic Flow-Measurement*. Cambridge, U.K.: Cambridge Univ. Press, 1962.

[15] J. Hemp, "A technique for low cost calibration of large electromagnetic flowmeters," *Flow Meas. and Instrumentation*, vol. 12, no. 2, pp. 123–134, 2001.

[16] K.-M. Lee, R. A. Sosseh, and Z. Wei, "Effects of the torque model on the control of a VR spherical motor," *IFAC Control Engineering Practice*, vol. 12/11, pp. 1437–1449, 2004.

[17] L. Yan, I.-M. Chen, G. Yang, and K.-M. Lee, "Analytical and experimental investigation on the magnetic field and torque of a permanent magnet spherical actuator," *IEEE/ASME Trans. Mechatronics*, vol. 11, no. 4, pp. 409–419, Aug. 2006.

[18] H. Son and K.-M. Lee, "Distributed multipole models for design and control of PM actuators and sensors," *IEEE/ASME Trans. Mechatronics*, vol. 13, no. 2, pp. 228–238, Apr. 2008.

[19] K.-M. Lee, K. Bai, and J. Lim, "Dipole models for forward/inverse torque computation of a spherical motor," *IEEE/ASME Trans. Mechatronics*, vol. 14, no. 1, pp. 46–54, Feb. 2009.

[20] K.-M. Lee, R. Roth, and Z. Zhou, "Dynamic modeling and control of a ball-joint-like VR spherical motor," *ASME J. Dynamic Syst., Meas. Control*, vol. 118, no. 1, pp. 29–40, 1996.

[21] J. H. Park and H.-W. Park, "A mesh-based disparity representation method for view interpolation and stereo image compression," *IEEE Trans. Image Processing*, vol. 15, pp. 1751–1762, 2006.

[22] N. M. Kwok, Q. P. Ha, D. Liu, and G. Fang, "Contrast enhancement and intensity preservation for gray-level images using multiobjective particle swarm optimization," *IEEE Trans. Autom. Sci. Eng.*, vol. 6, no. 1, pp. 145–155, Jan. 2009.

[23] J. W. Hwang and H. S. Lee, "Adaptive image interpolation based on local gradient features," *IEEE Signal Processing Lett.*, vol. 11, pp. 359–362, Mar. 2004.

[24] Q. Li and K.-M. Lee, "An adaptive meshless method for magnetic field computation," *IEEE Trans. Magn.*, vol. 42, no. 8, pp. 1996–2003, Aug. 2006.

[25] K.-M. Lee, Q. Li, and H. Sun, "Effects of numerical formulation on magnetic field computation using meshless methods," *IEEE Trans. Magnetics*, vol. 42, no. 9, pp. 2164–2171, Sep. 2006.

[26] *Adaptive Mesh Refinement – Theory and Applications*. New York: Springer, 2005.
[27] K.-M. Lee and S. Janakiraman, "A model-based vision algorithm for real-time flexible part-feeding and assembly," in *SME Applied Machine Vision Conf.*, Atlanta, GA, Jun. 1–4, 1992, Paper number: MS 92–211.

Liang Hu received the B.Eng. degree in 2004 from the Department of Mechanical Engineering, Zhejiang University, Hangzhou, China, and the Ph.D. degree in 2010 and currently works as a postdoctoral.

His current research interests include flow measurement and instrumentation, and measurement and computation of magnetic field.

Kok-Meng Lee (M'89–SM'02–F'05) received the B.S. degree from The State University of New York, Buffalo, in 1980, and the S.M. and Ph.D. degrees from the Massachusetts Institute of Technology, Cambridge, in 1982 and 1985, respectively.

He is currently a Professor with the Woodruff School of Mechanical Engineering, Georgia Institute of Technology, Atlanta. His current research interests include system dynamics/control, robotics, automation, and mechatronics. He holds eight patents in machine vision, 3-DOF spherical motor/encoder, and live-bird handling system.

Prof. Lee received the National Science Foundation Presidential Young Investigator Award, the Sigma Xi Junior Faculty Research Award, the International Hall of Fame New Technology Award, and the Kayamori Best Paper Award. He is a Fellow of the American Society of Mechanical Engineers.

Jun Zou received the Ph.D. degree from Zhejiang University, Hangzhou, China, in 2006.

He is an Associate Professor of Mechanical Engineering at Zhejiang University of China. He is author or coauthor of about 20 journal and conference papers and several patents. His current interests relate to flow rate measurement and applied fluid mechanics.

Xin Fu received the B.Eng. degree from Chengdu University of Science and Technology, Chengdu, China, in 1982, the M.Eng. degree from Southwest Agricultural University, Chongqing, China, in 1990, and the Ph.D. degree from the University of Leoben, Leoben, Austria, in 1999.

Since 1999, he has been with Zhejiang University, Hangzhou, China, where he was the Director of the State Key Laboratory of Fluid Power Transmission and Control from 2005 to 2009 and is currently a Professor and the Vice-Dean of the Department of Mechanical Engineering. His current research interests include microfluidic technology, simulation and visualization of flow field, fluid vibration and noise control, and flow measurement and instrumentation.

Hua-Yong Yang received the Doctorate degree in philosophy from the University of Bath, Bath, U.K., in 1988.

He is currently a Cheung Kong Scholar Chair Professor of Mechanical Engineering at the Zhejiang University of China. He has been the Director of the National Engineering Research Center of Electrohydraulic Control and also a committee member of the advanced manufacturing technology within the China High Technology 863 Program of the Ministry of Science and Technology (MOST) since 2000. He has been the chief scientist of a project supported by the National Basic Research Program of China since 2007. He is also the Editor of Chinese *Journal of Mechanical Engineering*. he has published one academic book and over 160 technical papers in national and international journals. He holds 65 China invention patents. His current research interests include motion control and energy saving of mechatronic systems, fluid power component and system development.

Dr. Yang is the recipient of the National Outstanding Researcher of the Natural Science Foundation of China Award. He is a Fellow of the Chinese Mechanical Engineering Society.